Correlation between dielectric, mechanical properties and electromechanical performance of functionalized graphene / polyurethane nanocomposites

Yan Zhang, L. Seveyrat, Laurent Lebrun

Correlation between dielectric, mechanical properties and electromechanical performance of functionalized graphene / polyurethane nanocomposites

Yan Zhang*, Laurence Seveyrat, Laurent Lebrun

Univ. Lyon, INSA-Lyon, LGEF, EA682, F-69621, Villeurbanne, France

Abstract:

Carbon-based electroactive polymers (EAPs) are core materials for actuator applications. Introducing conductive fillers into EAPs is considered an effective method to improve the actuating performance, due to the enhanced dielectric properties achieved. This work describes the elaboration and characterization of polyurethane (PU)/oxygen-functionalized graphene (OFG) composite films. Results revealed that for the nanocomposites, a large increase in dielectric constant was obtained without a great mechanical reinforcement, whereas there was no improvement in electromechanical performance as compared to pure polyurethane. The possible reasons for these discordant results were thus investigated with the help of multiscale studies. The importance of measuring the dielectric and mechanical properties under the same conditions as those used to drive actuators could be pointed out. Using high electric field values led to a better prediction of the electromechanical coefficient M_{31} for pure PU at low frequency, but did not completely explain the decreasing M_{31} found for the composites. The discrepancy could be due to the moderate adhesion between the polymer and the graphene nanoplatelets, but also to the competition between the increased dielectric constant and the decreased electric field seen by the polymer, induced by MWS interfacial polarization.

Keywords:

Graphene and other 2D-materials, Polyurethane, Polymer-matrix composites (PMCs), Electrical properties, Electromechanical behavior

* corresponding author: yan.zhang@insa-lyon.fr; +33 (0)4 72 43 89 92

1. Introduction

Electroactive polymers (EAPs) are used in a wide range of applications such as artificial muscles, sensors, microfluids and robotics, for their lightness, easy elaboration, and flexibility [1–4]. However, due to their relatively small dielectric constant, the application of EAPs are limited by the high driven electric field required. For this reason, research aiming at improving the electromechanical performance is of great interest [5–8]. Among the electronic EAPs, polyurethane (PU) is a promising candidate thanks to its low cost as well as balanced properties among which can be mention the electric field-induced strain, mechanical modulus and temperature behavior. The studied PU elastomer presented a specific structure with a mix of hard and soft segments. Thermodynamic incompatibility of the two types of segments led to a phase separation favoring a high-level electromechanical performance[7,9,10].

The total strain S can be expressed in terms of the Maxwell effect due to the electrostatic interaction between charged electrodes, and electrostriction, which is linked to the change in material properties with strain. The strain is related to the applied electric field E with a quadratic equation:

$$S = S_{Maxwell} + S_{electrostriction} = ME^2 \qquad (1)$$

A previous study on this polyurethane showed that the Maxwell effect is the main mechanism involved in the total strain [11]. Its electromechanical performance thus depends directly on the ratio of the dielectric constant (ε_r') to the mechanical Young's modulus (Y), so the electromechanical coefficient M_{31} can be expressed as [12]:

$$M_{31} = \frac{\varepsilon_0 \varepsilon_r'}{2Y} \qquad (2)$$

Consequently, increasing the dielectric constant is a convenient way to improve the performance of a PU actuator. Several approaches can be employed for this, including the incorporation of fillers. In the case of insulating fillers, large quantities are required which in turn gives rise to a significant increase in Y, to the detriment of M_{31}. For conductive fillers and especially nanosized ones, a lower content can be sufficient giving rise to a moderate mechanical

reinforcement. Many authors linked the beneficial effect of the conductive fillers to Maxwell-Wagner-Sillars interfacial polarization [13–15]. Consequently, it would be interesting to increase the quantity of interfaces by raising the filler content. The main issue is to preserve the insulating characteristic of the composite for which functionalization of the fillers can offer a suitable solution.

Research on composites of carbon nanotubes, graphene, carbon black have been reported for actuation applications [6,7,16,17]. Graphene is of particular interest, due to the extensive electron mobility and a large specific surface area in favor of interfacial polarization. Moreover, the functionalization of fillers favors the dispersion as well as the cohesion with the polymer matrix [18]. Therefore, in this work, oxygen-functionalized graphene nanoplatelets (OFG) were chosen to prepare PU/OFG composites.

An investigation was performed of the microstructural, mechanical and dielectric properties of PU/OFG nanocomposite films, in order to better understand how these properties affect the electromechanical coefficient M_{31}. Solution tape casting was used for the film elaboration. OFG weight contents were varied in the range 0-14.60 wt%. The impact of nanoplatelets on the PU microstructure was investigated by SEM and DSC analyses, and the dielectric and mechanical properties were characterized. Frequency, temperature and electric field ranges were chosen so as to separate the various mechanisms involved in the polyurethane properties, while considering the conditions for driving actuators. The electromechanical coefficients were evaluated by bender displacement measurements, and compared to the values calculated by equation (2). Their difference was discussed, especially in terms of conductivity/MWS relaxation contribution and the different dielectric behavior of PU and PU/OFG composites under a high electric field.

2. Experimental

2.1 Materials and preparation

Polyurethane granules (PU, Estane 58887 NAT 038, 1.13 g cm^{-3}, 87 shore A) and oxygen-functionalized graphene nanoplatelets (OFG, Graphene Supermarket, oxygen HDPlas^{TM}, planar size 0.3-5 µm, thickness <50 nm) were used to prepare PU/OFG composite films. The PU used in this work was a block copolymer, consisting of 4,4-methylene diphenyl diisocyanate (MDI), 1,4-butanediol (BDO) as hard segments, and poly(teramethylene) oxide (PTMO) as soft segments. Firstly, the PU granules were preheated at 80°C for 3 h following the recommendation of the supplier. Suitable content of OFG nanoplatelets were dispersed in N,N-dimethylformamide (DMF, Honeywell D158550) using an ultrasonic processor with a 7-mm sonotrode (Hielscher UP400S, amplitude 0.7, cycle 1, 40 min). Next, PU granules were dissolved in a DMF/OFG mixture with mechanical stirring and were heated at 80°C for 3h under reflux. The obtained homogenous solution (20 wt% PU in DMF) was left aside during 24 h after which the solution was applied to a glass plate by tape casting, followed by overnight heating at 60°C. A second treatment at 125°C for 3h was applied to remove the residual solvent and ensure the same thermal history. Films with a thickness of around 100 µm and a ratio of OFG to PU ranging from 0 to 14.60 wt% were finally obtained.

2.2 Microstructural characterization

The morphology of the PU/OFG composites was observed with a Zeiss Supra Scanning Electron Microscope (SEM) under high vacuum, at a low accelerating voltage of 1 kV. Observations were performed on cryofractured (cross-section) surfaces of the films.

Thermal properties were obtained with Differential Scanning Calorimetry (Setaram DSC 131 Evo) under a nitrogen atmosphere. A sample around 20 mg was encapsulated in a 120-µL aluminum crucible. It was first cooled down to -120 °C, then heated to 220 °C, and finally cooled down to ambient temperature. Heating and cooling ramps were carried out at a rate of 10 °C min^{-1}.

2.3 Mechanical characterization

The mechanical properties of the films were characterized by a setup consisting of a Newport translation table, a motion microcontroller (XPS), and a 10-N force sensor (Doerler Mesures LC102TC). Films with dimensions of 60 mm in length and 10 mm in width were held on one side with a fixed clamp and on the other side with a mobile clamp, with and without the application of an electric field (function generator, amplifier trek 10/10). A low strain of 1 % was applied to the samples at a speed of 0.4 % s^{-1}. The strain as well as the stress response of the samples was detected by the motion controller and the force sensor. The Young's modulus of the composite films (Y) was determined on the linear part of the curve from the ratio of stress to strain.

2.4 Dielectric characterization

Gold electrodes (20 mm diameter, 26 nm thickness) were coated on both surfaces of the films by sputtering (Cressington 208HR). Dielectric spectroscopy was carried out using a Schlumberger Solartron 1255 impedance/gain phase analyzer and a 1296 dielectric interface. The dielectric constant and conductivity were determined in the frequency range of 0.1Hz - 1MHz.

Temperature measurements were performed under liquid nitrogen using a cryostat (Optistat DN2 Oxford Instruments) and a temperature controller (Oxford ITC503). Measurements were performed in a temperature range of 180-350 K and a frequency range of 0.1 Hz - 1MHz, at 1 V_{RMS}.

The dielectric constant was also recorded at high levels of electric field in the range 0.7-10 MV m^{-1} at 0.1 Hz. A unipolar AC voltage was generated by the impedance/gain phase analyzer, amplified by a Trek 10/10 amplifier, and applied to the sample.

2.5 Electromechanical characterization

The composite films were coated with a 26-nm gold electrode on both surfaces, and then attached to a rigid substrate (Mylar, RS 785-0792, 100 µm) with double-sided tape (3M, ATG

969, 100 µm). The electromechanical coefficient M_{31} of the obtained cantilever was evaluated with the help of a laboratory-built characterization bench (Fig. 1).

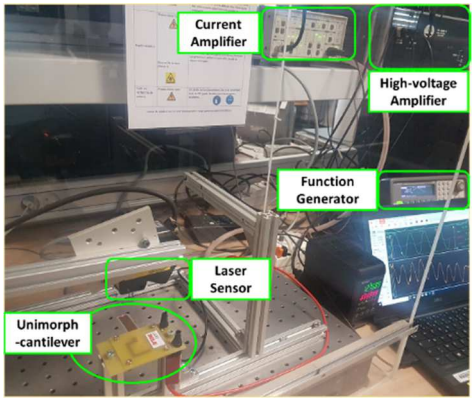

Fig. 1. Setup for the measurement of the electromechanical coefficient M_{31}.

One end of the unimorph cantilever structure was clamped in the device, with the other end free to move. The active area was 40 mm x 10 mm x 0.1 mm. A unipolar AC electric field of 10 MVm^{-1} at 0.1 Hz was applied to the sample with the help of a function generator (Agilent 33220A) and a high-voltage amplifier (Trek 609-6). When the electric field was applied, a transverse elongation was generated in the polymer film, forcing the cantilever to bend. The tip displacement δ of the free end was measured by a laser sensor (3RG7056-3CM00-PF Pepperl+Fuchs), and the field-induced strain S_{31} could then be calculated from the measured displacement δ, with consideration taken to the configuration geometry and material properties. The M_{31} coefficient was deduced from S_{31}. Details of the calculations can be found in [11].

At least four samples of each composition were used for the dielectric, mechanical and electromechanical measurements, except for the thermally dependent dielectric measurements.

3. Results and discussions

3.1 Microstructure of PU and PU/OFG composites

Fig. 2 presents an example from the SEM analysis of the composite containing 10.25 wt% of OFG.

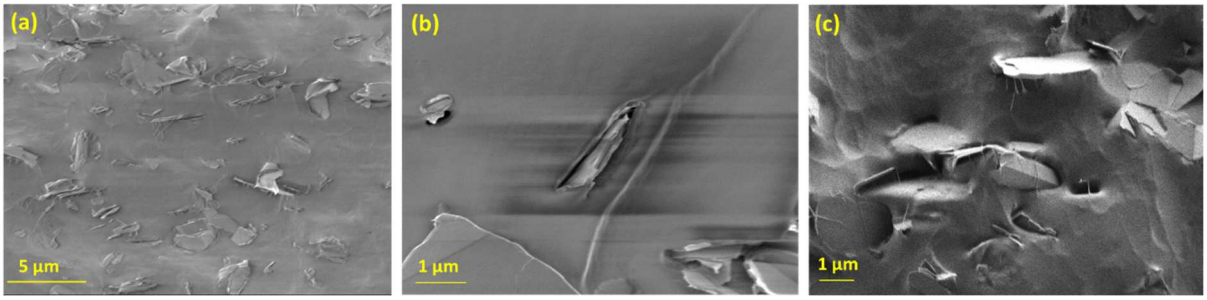

Fig. 2. SEM micrographs of a cryofractured (cross section) surface of the PU-10.25 wt%-OFG.

According to Fig. 2(a), the OFG nanoplatelets were overall uniformly distributed in the PU matrix. There was no sign of a preferential orientation of the nanoplatelets: they exhibited various orientations and positions (platelets in and perpendicular to the plane), indicating a three-dimensional (3D) distribution in the PU matrix. Fig. 2(b) displays a stack of a few OFG nanoplatelets (about 200 nm in thickness). The cohesion between the stacked platelets and the polymer appeared to be imperfect since the cryofracture created a gap between them. In addition, Fig. 2(c) confirms this observation by highlighting a few links between the OFG nanoplatelets and the PU matrix, though the interfacial cohesion was incomplete.

The planar size (l) and thickness (d) of the OFG nanoplatelets were determined statistically from the SEM analysis. A planar size of 1.56± 0.64 µm and a thickness of 115± 83 nm were obtained. The planar size was in the range given by the supplier, while the thickness was greater than 50 nm, in agreement with the observed stacked platelets. The mean aspect ratio (A_f= l/d) was 14.

Fig. 3 depicts an example of DSC thermograms for PU and a PU/OFG composite. The thermal properties of all the compositions are given in Table 1.

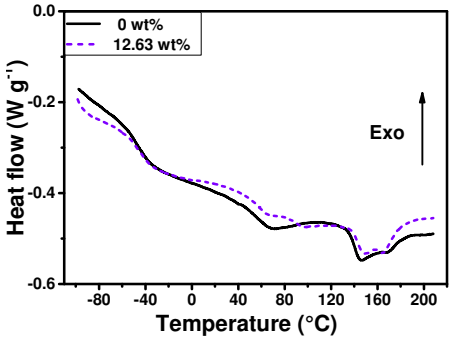

Fig. 3. DSC thermograms of PU and PU-12.63 wt%-OFG.

Table 1. Thermal properties of PU-OFG films from DSC experiments.

wt% OFG	Tg_{SS} (°C)	ΔCp (mW)	T_{m1-2} (°C)	ΔH_f (J/g)
0	-50.0	1.2	147-169	12.8
2.77	-45.2	1.3	147-169	13.1
5.40	-48.9	1.3	150-168	11.6
10.25	-47.5	1.1	147-170	12.6
12.63	-45.8	1.2	150-169	11.2
13.13	-41.1	1.1	147-173	11.2

Four main thermal events could be observed during the temperature evolution. The first thermal event at -40/-50°C was related to the glass transition of the soft segments (SS) in PU, giving an indication of the separation state between soft and hard segments (HS). Globally, the Tg values did not vary considerably with the OFG content: only a moderate increase was noted at high contents. This increase could be an indication of a higher quantity of HS dissolved in the soft domains and thus a higher degree of HS-SS mixing [19]. The endotherm in the range 40-80°C, which can be associated to local restructuring of HS units within the hard micro-domains [20] was not affected by the presence of OFG even if a slight modification was observed with OFG contents of 12.63 wt% and 13.13 wt%.

There were two possible interpretations for the bimodal endotherm (T_{m1} and T_{m2}) in the range 130-180°C. The first one was the micro-mixing of non-crystalline or semi-crystalline hard and soft phases followed by the fusion of crystalline HS [20]. The second was the fusion of crystalline HS with the two peaks related to two lengths of HS [19]. In both cases, the increase of the crystallinity was linked to an increase of T_{m1} and T_{m2} and the global melting enthalpy ΔH_f. In our case, the crystallinity could be considered to be unchanged, since the ΔH_f was almost constant versus the OFG content, and no significant change of the T_{m1} nor T_{m2} value was observed.

3.2 Mechanical properties

Fig. 4(a) gives an example of a stress-strain curve of the PU/OFG composites. Fig. 4(b) presents the experimental Young's modulus versus OFG content.

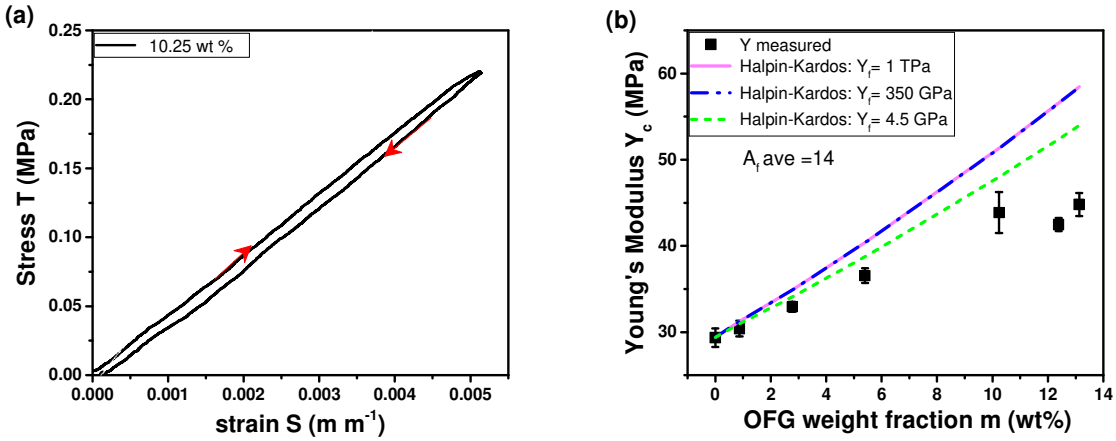

Fig. 4. (a) Stress-strain curve of PU-10.25 wt% OFG at a speed of 0.1 % s^{-1}, (b) the Young's modulus of the PU and PU/OFG composites measured and predicted by the Halpin-Kardos model with varying Y_f values.

Due to the nature of the OFG fillers (nanoplatelets) and its random dispersion, the Halpin-Kardos model was chosen to predict the Young's modulus according to (3):

$$\frac{Y}{Y_m} = \frac{3}{8}\frac{(1+2A_f\mu_L\phi_f)}{(1-\mu_L\phi_f)} + \frac{5}{8}\frac{(1+2\mu_T\phi_f)}{(1-\mu_T\phi_f)} \qquad (3)$$

where Y and Y_m are the Young's Modulus of respectively the composites and the matrix, Φ_f is the volume fraction of fillers, which was calculated assuming a density of 2.2 g cm^{-3} for OFG and 1.13 g cm^{-3} for PU, A_f is the aspect ratio, whose average value was determined to be 14 earlier in this work, and μ_L and μ_T are geometry factors, according to (4) and (5).

$$\mu_L = \frac{Y_f/Y_m - 1}{Y_f/Y_m + 2A_f} \qquad (4)$$

$$\mu_T = \frac{Y_f/Y_m - 1}{Y_f/Y_m + 2} \qquad (5)$$

Here, Y_f is the Young's modulus of the fillers. This model assumes that a perfect adhesion between polymer and filler.

Both the experimental and predicted values increased linearly with the introduction of OFG, and the predicted values were reasonably close to the experimental ones. The increase in

Young's modulus with the OFG content was moderate. For example, an increase of 30 % was obtained with 10.25 wt% OFG loading. As there was an uncertainty regarding the Y_f due to the fact that the Young's modulus usually decreases with the number of graphene layers due to the slippage between the layers [21], 3 values were employed for the model: 1 TPa for a monolayer [22], 350 GPa as published for a 10-layer graphene sample [23] and for the lowest value of 4.5 GPa corresponding to the Young's modulus of graphite [24].

Among the possible physical values for Y_f, the best fit was obtained for the lowest value. Possible reasons can be the decrease of Y_f induced by the functionalization, as reported in literature [25], and the moderate interfacial adhesion between the polymer and the nanoplatelets, which is in good agreement with the SEM micrographs. This effect was indeed not considered by the model, and consequently, the mechanical reinforcement was moderate, in favor of a large electric field-induced strain.

3.3 Dielectric properties

Fig. 5(a) presents the evolution of the real part of the dielectric constant (ε_r') for different OFG weight fractions (m) as a function of the frequency for PU films and PU-OFG nanocomposites.

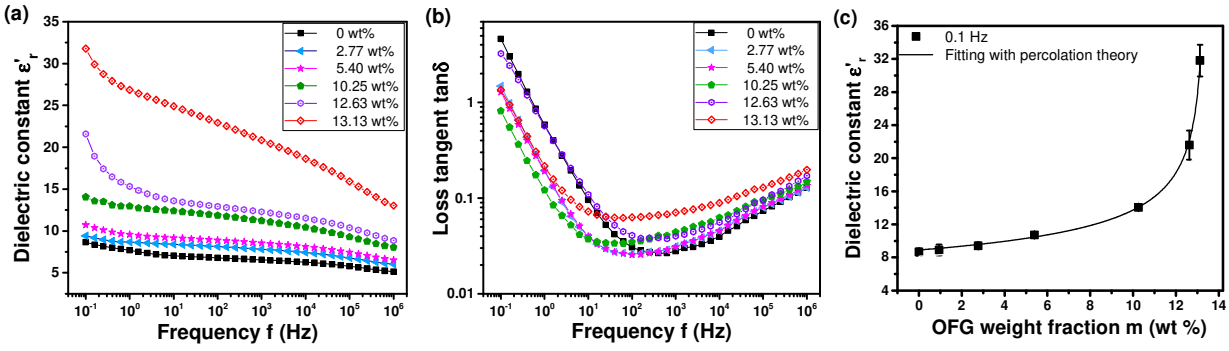

Fig. 5. (a) Variation of the real part of the dielectric constant ε_r' and (b) the loss factor tanδ as a function of frequency, (c) the dielectric constant ε_r' versus OFG weight fraction.

The dielectric constant decreased when the frequency increased for both the PU film and the PU/OFG composites. Two slope changes were observed: the first one occurred at the lowest frequencies and is usually attributed in the literature to different phenomena such as DC

conduction, Maxwell Wagner Sillars (MWS) polarization and/or electrode polarization[8,17,26]; and the second one, less pronounced, around 10^4 Hz, generally attributed to dipolar relaxation.

Figure 5(b) depicts the variation of the loss tangent (ratio of the imaginary part ε_r" to the real part ε_r' of the dielectric constant) versus frequency for various OFG contents. As for the pure PU films, as the frequency increased, the nanocomposites exhibited a large decrease in loss tangent followed by a moderate increase. The decrease observed for low frequencies was linked to the end of the contribution of electrode polarization, MSW polarization and/or conduction to the dielectric properties whereas the increase at medium frequencies was due to other dipolar relaxations. For frequencies below 10 Hz, lower loss tangent values were obtained for all composites as compared to pure PU.

Generally, conductive fillers increase the loss tangent of the composites [7,16,17]. Only very few papers have reported on lower dielectric losses with conductive fillers [27]. This decrease could certainly be associated to the functionalization of graphene. The insulating layer formed by the plasma functionalization may have played an effective role since the oxygen functionalization created carbonyl, hydroxyl and other functionalities on the surface of the conductive platelets.

Fig. 5(c) presents the variation of the dielectric constant versus OFG content, at 0.1 Hz. The dielectric constant increased with the OFG content and this occurred to a greater extent after 10.25%. The attained value of the dielectric constant was about four times higher than that of the PU film.

Below the percolation threshold, the experimental data can be modeled by [33]:

$$\varepsilon_r' = \varepsilon_{rm}'(1 - \frac{m}{m_c})^{-q} \qquad (6)$$

Here, ε_{rm}' is the dielectric constant of the polymer matrix, m_c is the percolation threshold, and q is the critical exponent.

At 0.1 Hz, a percolation threshold of 13.34 wt% and a q exponent of 0.32 were obtained. This percolation threshold was situated in the upper part of the percolation rate range reported for

composites with conductive fillers [28]. According to the literature, typical values for the q exponent are 1, 1.3 and 0.7 for 1D, 2D and 3D space dimensions[29–32], respectively. q values below 0.5 have also been reported and attributed to a 3D network of fillers [33]. The q value of 0.32 obtained in this work can be related to a 3D distribution of OFG nanoplatelets, which was confirmed by the SEM micrograph.

Fig. 6(a) presents the real part of the conductivity (σ') of PU and PU/OFG composites as a function of the angular frequency (ω). The curve of conductivity of both PU and PU/OFG composites consisted of two parts, namely, a low-frequency plateau, followed by a monotonously increasing part at higher frequency. In this higher frequency range, the conductivity increased when raising the OFG content, which was consistent with higher conduction values of the graphene fillers. For concentrations beyond 14.60%, the global conductivity exhibited a sharp increase in accordance with a percolating system.

According to Jonscher's law[34], the conductivity σ' can be described as:

$$\sigma' = \sigma_{DC} + A\omega^{n} \qquad (7)$$

where A is a constant and n is the power exponent.

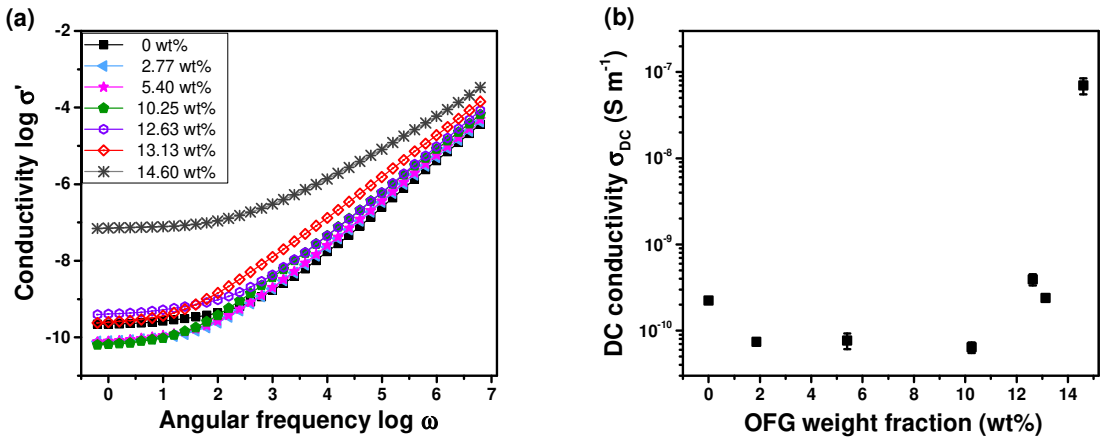

Fig. 6. (a) Conductivity of PU/OFG composites versus frequency, (b) DC conductivity versus OFG weight fraction.

The DC conductivity σ_{DC} corresponds to the value measured for the plateau. The n exponent was obtained using the slope of the curve representing log ($\sigma' - \sigma_{DC}$) as a function of log ω (data

not shown). The n exponent was in the range 1 to 1.1, except for 14.60 wt% with n near 0.8. Despite that the exponent is limited to $n \leq 1$ in the original Jonscher's law, reports on n values higher than unity exist in polymers with ionic-like conduction mechanisms [35,36]. For a higher OFG content near the percolation threshold, the n exponent value diminishes which can indicate the contribution of electronic hopping conduction.

Fig. 6(b) depicts the evolution of σ_{DC} versus the OFG content. The observed trend was similar to that obtained for the loss tangent: an initial decrease for low and moderate OFG contents followed by an increase for higher contents in the vicinity of the percolation threshold. The evolution was therefore quite different from what has been described in several papers on EAP composites with carbon fillers [17,37], which reported a monotonic increase of DC conductivity when increasing the content of conductive fillers. Since σ_{DC} is related to the transport of free charges from one electrode to another, it can be assumed that the OFG would behave as traps for the charged mobile species with an efficiency correlated to the distance between them. In addition, the isolating layer created by the functionalization can also contribute to the decrease of the conductivity, as it did for loss tangent. For a moderate OFG content, the distance between two neighboring traps was high enough to disturb the charge transport but this capability decreased as the distance was reduced, thus leading to new paths for the charge displacement. Near the percolation threshold, an electronic conduction can have an important role through the tunnel effect.

Temperature-dependent experiments were conducted for a more thorough interpretation of the charge carrier transport in these materials. It was important to pay particular attention to these features since they occur near room temperature and can help with the interpretation of the electromechanical performance of such EAPs.

Fig. 7 presents the evolution of the imaginary part of the dielectric constant ε_r" and the modulus M" in the temperature range from -100 to 80 °C. The dielectric modulus M" formalism [38] (equation (8)) can be used to highlight relaxation phenomena not observed with ε_r",

especially at low frequencies when high dielectric constant and conductivity values can mask the phenomena.

$$M^{"} = \frac{\varepsilon_r^{"}}{\varepsilon_r'^2 + \varepsilon_r^{"2}} \qquad (8)$$

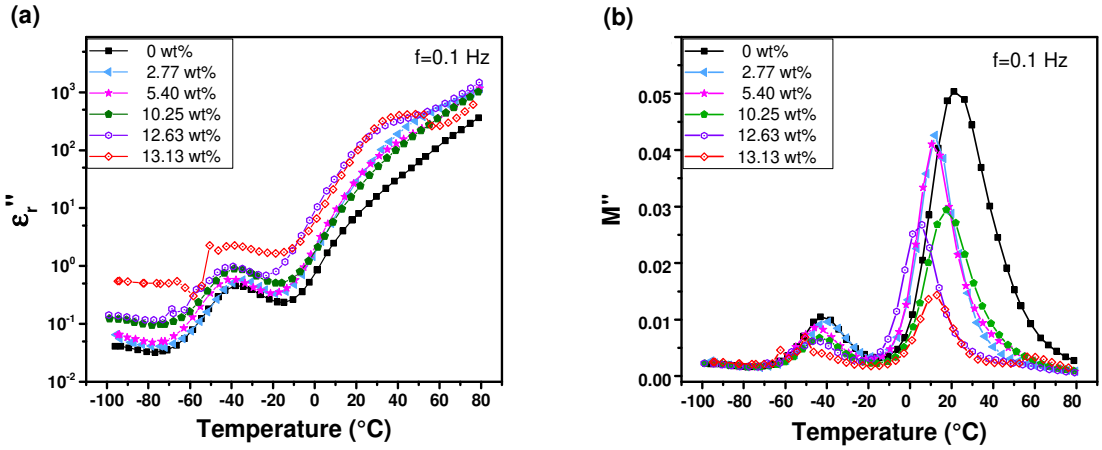

Fig. 7. Dielectric relaxations of PU/OFG composites at 0.1 Hz (a) imaginary part of the dielectric constant ε_r", (b) imaginary part of the dielectric modulus M".

Two maxima of M" were clearly observed for the PU and the PU/OFG composites. Another peak of lower intensity was also present near -90 °C, assigned to the β-relaxation caused by the local motion of polar groups on the polymer chain. This relaxation was not really affected by the OFG nanoplatelets. The second peak around -50/-40 °C was related to the α-relaxation with the segmental motion of the soft phase. The polymer went from a rubbery to a glassy state. The PU and nanocomposites exhibited similar positions for the α-relaxation, in agreement with the Tg values obtained by DSC. The β and α relaxations are well documented for polyurethanes [39,40], and are not affected by fillers. In addition, the temperature range is below that used for actuators. For all these reasons, attention was paid to the last peak in the vicinity of room temperature. This peak was highly dependent on OFG content, with the position of the maximum varying from 0 to 25 °C. A mix of interfacial polarization (MWS), conduction and/or electrode polarization was associated to this range. To go deeper in the interpretation and obtain information on the type of charges involved in this process, two studies were conducted: the variation of DC conductivity

with temperature, and the treatment of the relaxation phenomena in the range from -10°C to 35°C after subtracting the σ_{DC} part.

Fig. 8(a) presents the evolution of the log of σ_{DC} versus 1/T. In the temperature range -10 °C to 35 °C, log σ_{DC} exhibited a near linear relation with 1/T. The temperature range was chosen so as not to consider other phenomena such as the α relaxation. The linear evolution agreed with the Arrhenius law:

$$-log\sigma_{DC}(T) = log\sigma_0 + \frac{E_a}{K_B T} \qquad (9)$$

where σ_0 is the pre-exponential factor, E_a is the activation energy of DC conduction, and K_B is the Boltzman constant.

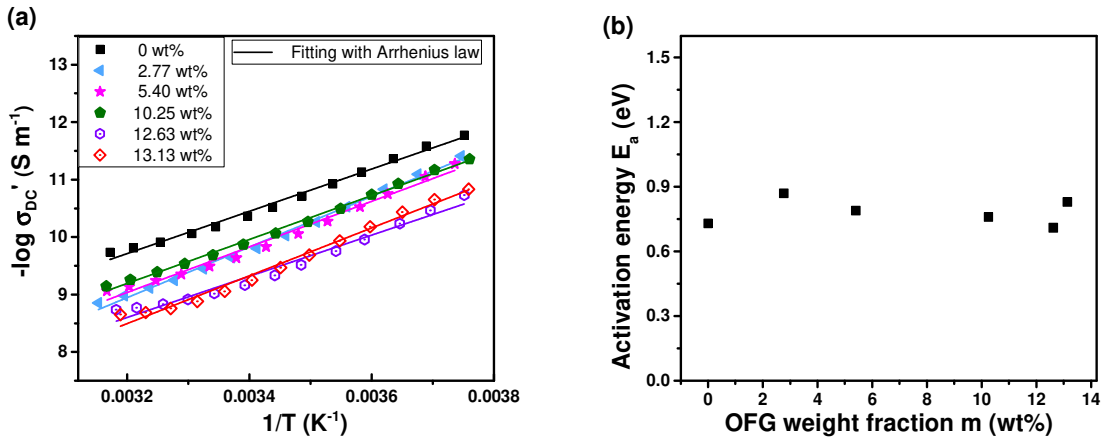

Fig. 8. Evolution of the DC conductivity of PU and the PU/OFG composites: (a) log σ_{DC} versus 1/T, (b) activation energy versus OFG content.

Fig. 8(b) presents the evolution of the activation energy as a function of the OFG content. It was in the range 0.7- 0.9 eV, regardless of the OFG content. These two observations favored the idea of an ionic conduction.

Fig. 9(a) depicts the evolution of ε_r" versus the angular frequency for various contents of OFG. The contribution of the conductivity ($\sigma_{DC}/\varepsilon_0\omega$) on ε_r" was then subtracted from the measured values to remove the ohmic conduction part in the loss spectra ε_r". Fig. 10(b) presents the obtained values.

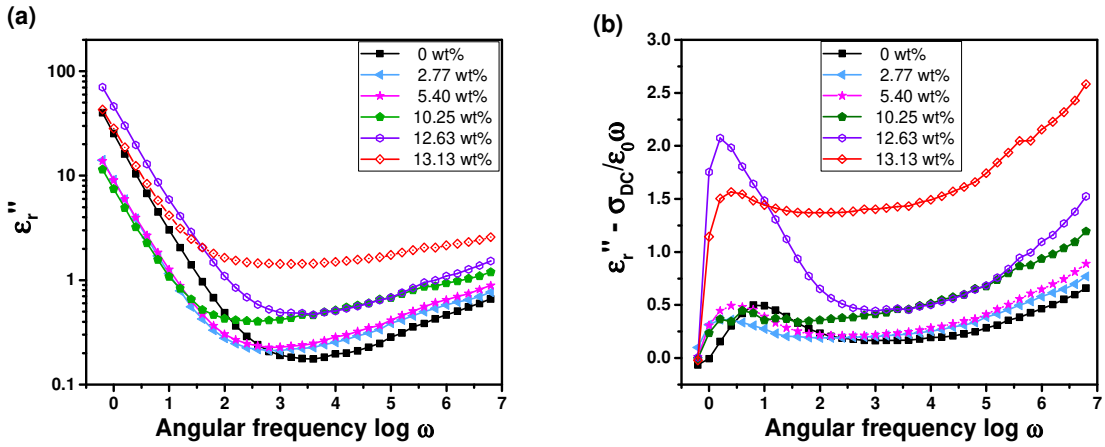

Fig. 9. Evolution of (a) the imaginary part of the dielectric constant ε_r" and (b) ε_r" without the DC conduction part versus angular frequency.

Relaxation peaks were visible in the corrected spectra, revealing the MWS relaxation. They were fitted using the double stretched Havriliak-Negami relaxation function[41]:

$$\varepsilon^*(\omega) = \varepsilon_\infty + \frac{\Delta\varepsilon}{[1+(i\omega\tau)^\alpha]^\beta} \qquad (10)$$

where ε_∞ is the dielectric constant at high angular frequency far from the relaxation peak, $\Delta\varepsilon$ is the dielectric dispersion, τ is the characteristic relaxation time, and α and β are related to the asymmetry and broadness of the spectra, respectively. The Havriliak-Negami fitting results on conduction-free loss relaxation are presented in Fig. 10 at ambient temperature (298 K).

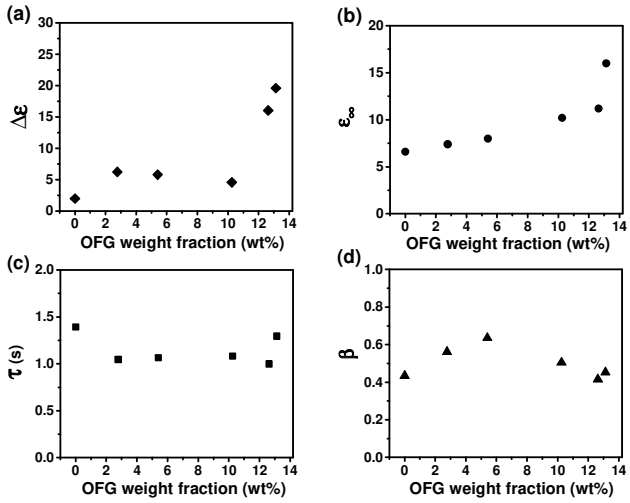

Fig. 10. Havriliak-Nagami fitting parameters versus OFG content for the MWS relaxation at ambient temperature (from DC conduction-free dielectric data): (a) dielectric dispersion $\Delta\varepsilon$, (b) high frequency dielectric constant ε_∞, (c) relaxation time τ, (d) spectra broadness parameter β.

The dielectric dispersion Δε increased non-linearly with the OFG content, going from 2 for the pure PU to 5-6 for low and moderate OFG contents, and then abruptly grew for contents in the vicinity of the percolation threshold. This was evidence of a MWS polarization contribution non-proportional to the OFG content, and it was consequently indirectly correlated to the number of interfaces. ε_∞ presented a slight increase versus OFG content, indicating that contrarily to what is generally assumed other relaxations, such as α and β relaxations, may have contributed. This point is currently under investigation.

The relaxation time τ remained in the range 1.0-1.5 s, and was not significantly influenced by the OFG content. The parameter α was equal to 1 for all the compositions, evidencing that the distribution of the relaxation time was symmetric, whereas the β parameter lay in the range 0.4-0.65, displaying a significant broadness of the distribution. Both for PU and the PU/OFG composites, the MWS polarization did not relax at a single frequency. From the temperature dependence of the relaxation time (data not shown), the activation energy was determined to be in the range 0.1-0.35 eV. The E_a was not greatly affected by the OFG content and the low values obtained indicated a high dipole mobility.

3.4 Electromechanical properties

Figure 11 depicts the variation of S_{31} versus the square of electric field amplitude for PU and composites. As expected for Maxwell effect, a linear increase of S_{31} was observed, allowing the calculation of M_{31} with the slope of the curve. The electrical breakdown was estimated to be over 25 MV^{-1} for all compositions.

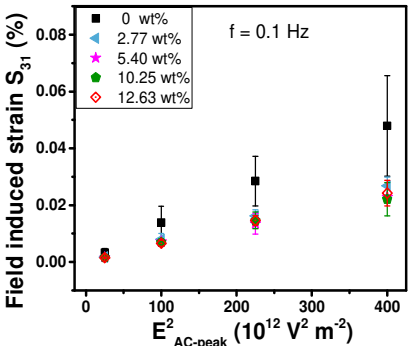

Fig. 11. Field-induced strain S_{31} versus square of electric field, at 0.1 Hz and 5-20 MV m^{-1}.

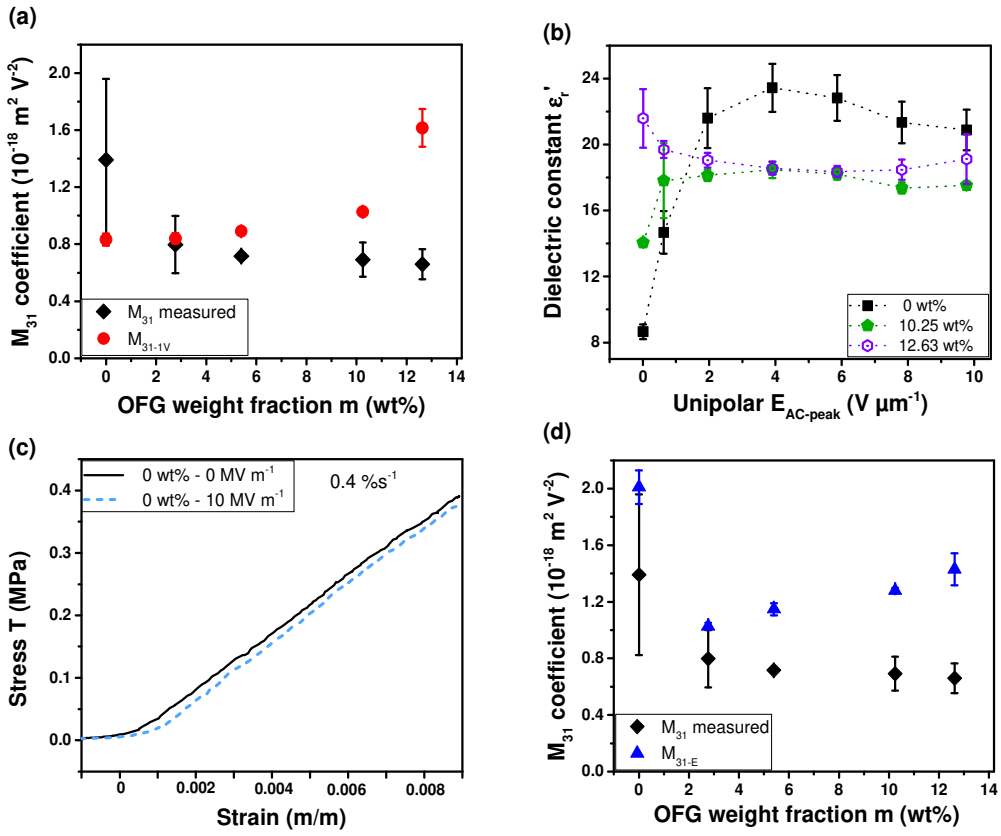

Fig. 12. (a) M_{31} of PU/OFG composites measured at 10 MV m^{-1}, 0.1 Hz and M_{31} calculated with equation (2), (b) evolution of the dielectric constant of PU and PU/OFG composites versus electric field, (c) strain-stress curve of PU with/without an electric field applied, (d) M_{31} of PU/OFG composites measured and calculated with ε_r' and Y obtained at 10 MV m^{-1}, 0.1 Hz.

Fig. 12(a) depicts the evolution of the measured M_{31} and predicted $M_{31\text{-}1V}$ (from the dielectric constant and Young's modulus recorded at 1 V_{RMS}) versus the OFG content at 0.1 Hz.

The predicted $M_{31\text{-}1V}$ increased with the filler content, first at a moderate level and then more dramatically near the percolation threshold. This is in good agreement with the large increase of the dielectric constant, which is more important than the increase of Young's modulus. The evolution of the measured M_{31} exhibited a different trend. The measured M_{31} values of the composites were lower than the ones of pure PU, and it decreased slightly with the OFG content. The measured M_{31} values of pure PU were highly dispersed. It is noteworthy that the measurement conditions in terms of temperature and frequency were also those where a very large variation of dielectric properties was observed.

The inability of the ε_r'/Y law to predict the measured data can also be linked to the fact that the dielectric constant and the Young's modulus can depend on the electric field. Given that EAPs work at electric fields from a few to hundreds of MV m^{-1}, it was essential to investigate the dielectric and mechanical properties under high electric fields.

Fig. 12(b) presents the evolution of the real part of the dielectric constant as a function of applied electric field for PU and two composites at 0.1 Hz. Their dielectric behavior was different: the dielectric constant of the pure PU was three-fold of that at moderate electric fields before stabilizing at a value near 20 at 10 MV m^{-1}. The increase was lower for PU-10.25wt%-OFG, and for PU-12.63wt%-OFG, a decrease was observed.

Fig. 12(c) presents an example of a strain-stress curve, measured with and without a 10-MV m^{-1} electric field for pure PU. The curves without and with an electric field were parallel, indicating that the electric field had no influence on the Young's modulus.

The evolution of the measured M_{31} coefficients and new predicted values of M_{31} from data measured at 10 MV m^{-1} (namely $M_{31\text{-}E}$) were then plotted and can be seen in Fig. 12(d). The $M_{31\text{-}E}$ coefficient was successful in predicting the higher M_{31} of pure PU compared to the composites, while $M_{31\text{-}1V}$ did not. For the PU/OFG composites, neither $M_{31\text{-}1V}$ nor $M_{31\text{-}E}$ were able to predict the measured coefficients, or the decrease in measured M_{31} versus OFG content. The difference between the experimental and calculated coefficients increased with the OFG content. This observation can be correlated with the increase in $\Delta\varepsilon$ and ε_∞ parameters due to the MWS relaxation. The depolarizing field induced by the interfacial polarization could indeed diminish the applied field, leading to a competition between the increase in dielectric constant and the effective electric field seen by the polymer.

In addition, fluctuations in the temperature range harboring the maximum of the relaxation peak could produce strong variations in dielectric properties, leading to a dispersion of the measured M_{31}. As discussed previously in this paper, the moderate mechanical interfacial adhesion could also affect the strain transmission and reduce the macroscopic electric field-

induced strain.

4. Conclusions

The mechanical, dielectric and electromechanical properties of PU/OFG composites with various OFG content were investigated, with attention paid to the properties at low frequency and temperatures between -20 and 35°C, where most EAP actuators and energy harvesters work.

The 3D distribution of nanoplatelets in the composites was confirmed by SEM analysis as well as the percolation law. The mechanical reinforcement remained modest probably due to a moderate adhesion between polymer and graphene nanoplatelets, highlighted by SEM and in agreement with over-estimated values predicted from the Halpin-Kardos model.

DSC experiments revealed that the microstructure of polyurethane was not really affected by the presence of functionalized graphene, indicating the extrinsic role of the fillers on the properties.

As excepted, a large increase of the dielectric constant was obtained near the percolation threshold, as well as a decrease versus frequency. The variation in DC conductivity versus OFG content supported the fact that the OFG behaved as traps for the charged mobile species with the efficiency correlated to the distance between traps. The obtained activation energy lay in a range 0.7- 0.9 eV, regardless of the OFG content, pointing at an ionic origin of the conduction.

A detailed study was carried out on the dielectric relaxation peak at low frequency, near room temperature, after removing the contribution of the DC conduction. Havriliak-Negami fitting indicated a Maxwell Wagner Sillars polarization contribution. It was however not proportional to the OFG content, and consequently not directly correlated to the number of interfaces.

A comparison of the experimentally determined M_{31} and the calculated M_{31} revealed the importance of taking the dielectric constant values under the same conditions as those used to drive actuators. The dielectric constant measured at high electric fields gives a better prediction of the electromechanical coefficient M_{31} of pure PU at low frequency, but does not completely explain the decreasing M_{31} of the composites. A possible explanation for this could be that the

interfacial polarization decreased the electric field seen by the composites and counterbalanced the increase in dielectric constant. Other factors, such as a moderate mechanical interfacial adhesion as well as temperature fluctuations around the maximum of the relaxation peak, could also explain the values of the M_{31} coefficients.

Acknowledgement

The Authors thank the Centre Lyonnais de Microscopy (CLYM) for the SEM analysis. Yan Zhang thanks the China Scholarship Council for financial support during her PhD studies.

References

[1] F. Carpi, I. Anderson, S. Bauer, G. Frediani, G. Gallone, M. Gei, C. Graaf, C. Jean-Mistral, W. Kaal, G. Kofod, M. Kollosche, R. Kornbluh, B. Lassen, M. Matysek, S. Michel, S. Nowak, B. O'Brien, Q. Pei, R. Pelrine, B. Rechenbach, S. Rosset, H. Shea, Standards for dielectric elastomer transducers, Smart Mater. Struct. 24 (2015) 105025. https://doi.org/10.1088/0964-1726/24/10/105025.

[2] D. Chen, Q. Pei, Electronic Muscles and Skins: A Review of Soft Sensors and Actuators, Chem. Rev. 117 (2017) 11239–11268. https://doi.org/10.1021/acs.chemrev.7b00019.

[3] R. Pelrine, R.D. Kornbluh, Q. Pei, S. Stanford, S. Oh, J. Eckerle, R.J. Full, M.A. Rosenthal, K. Meijer, Dielectric Elastomer Artificial Muscle Actuators: Toward Biomimetic Motion, Smart Struct. Mater. 4695 (2002) 126–137. https://doi.org/10.1117/12.475157.

[4] Y. Bar-Cohen, Q.M. Zhang, Electroactive polymer actuators and sensors, MRS Bull. 33 (2008) 173–177. https://doi.org/10.1557/mrs2008.42.

[5] L.J. Romasanta, M.A. Lopez-Manchado, R. Verdejo, Increasing the performance of dielectric elastomer actuators: A review from the materials perspective, Prog. Polym. Sci. 51 (2015) 188–211. https://doi.org/10.1016/j.progpolymsci.2015.08.002.

[6] M. Panahi-Sarmad, B. Zahiri, M. Noroozi, Graphene-based composite for dielectric elastomer actuator: A comprehensive review, Sensors Actuators A Phys. 293 (2019) 222–

241. https://doi.org/10.1016/j.sna.2019.05.003.

[7] K. Wongtimnoi, B. Guiffard, A. Bogner-Van de Moortèle, L. Seveyrat, C. Gauthier, J.Y. Cavaillé, Improvement of electrostrictive properties of a polyether-based polyurethane elastomer filled with conductive carbon black, Compos. Sci. Technol. 71 (2011) 885–892. https://doi.org/10.1016/j.compscitech.2011.02.003.

[8] F. Carpi, G. Gallone, F. Galantini, D. De Rossi, Silicone-poly(hexylthiophene) blends as elastomers with enhanced electromechanical transduction properties, Adv. Funct. Mater. 18 (2008) 235–241. https://doi.org/10.1002/adfm.200700757.

[9] I. Diaconu, D. Dorohoi, Properties of polyurethane thin films, J. Optoelectron. Adv. Mater. 7 (2005) 921–924.

[10] G. Diguet, A. Bogner, J.M. Chenal, J.Y. Cavaille, Physical modeling of the electromechanical behavior of polar heterogeneous polymers, J. Appl. Phys. 112 (2012) 114905. https://doi.org/10.1063/1.4766280.

[11] Y. Zhang, V. Perrin, L. Seveyrat, L. Lebrun, On a better understanding of the electromechanical coupling in electroactive polyurethane, Smart Mater. Struct. 29 (2020) 055007. https://doi.org/10.1088/1361-665X/ab7947.

[12] I. Kracovsky, T. Romijn, A few remarks on the electrostriction of elastomers, J. Appl. Phys. 85 (1999) 628–629. https://doi.org/10.1063/1.369418.

[13] T.H.T. Fook, J.H. Jeon, P.S. Lee, Transparent flexible polymer actuator with enhanced output force enabled by conductive nanowires interlayer, Adv. Mater. Technol. 5 (2020) 1–9. https://doi.org/10.1002/admt.201900762.

[14] G.M. Tsangaris, G.C. Psarras, N. Kouloumbi, Electric modulus and interfacial polarization in composite polymeric systems, J. Mater. Sci. 33 (1998) 2027–2037. https://doi.org/10.1023/A:1004398514901.

[15] H. Sun, H. Zhang, S. Liu, N. Ning, L. Zhang, M. Tian, Y. Wang, Interfacial polarization and dielectric properties of aligned carbon nanotubes/polymer composites: The role of

molecular polarity, Compos. Sci. Technol. 154 (2018) 145–153. https://doi.org/10.1016/j.compscitech.2017.11.008.

[16] C. Park, J.H. Kang, J.S. Harrison, R.C. Costen, S.E. Lowther, Actuating single wall carbon nanotube-polymer composites: Intrinsic unimorphs, Adv. Mater. 20 (2008) 2074–2079. https://doi.org/10.1002/adma.200702566.

[17] Q. Li, Q. Xue, L. Hao, X. Gao, Q. Zheng, Large dielectric constant of the chemically functionalized carbon nanotube/polymer composites, Compos. Sci. Technol. 68 (2008) 2290–2296. https://doi.org/10.1016/j.compscitech.2008.04.019.

[18] T. Ramanathan, A.A. Abdala, S. Stankovich, D.A. Dikin, M. Herrera-Alonso, R.D. Piner, D.H. Adamson, H.C. Schniepp, X. Chen, R.S. Ruoff, S.T. Nguyen, I.A. Aksay, R.K. Prud'Homme, L.C. Brinson, Functionalized graphene sheets for polymer nanocomposites, Nat. Nanotechnol. 3 (2008) 327–331. https://doi.org/10.1038/nnano.2008.96.

[19] D.J. Martin, G.F. Meijs, G.M. Renwick, S.J. McCarthy, P.A. Gunatillake, The effect of average soft segment length on morphology and properties of a series of polyurethane elastomers. I. Characterization of the series, J. Appl. Polym. Sci. 62 (1996) 1377–1386. https://doi.org/10.1002/(sici)1097-4628(19961128)62:9<1377::aid-app7>3.3.co;2-5.

[20] J.T. Koberstein, T.P. Russell, Simultaneous SAXS-DSC study of multiple endothermic behavior in polyether-based polyurethane block copolymers, Macromolecules. 19 (1986) 714–720. https://doi.org/10.1021/ma00157a039.

[21] C. Lee, X. Wei, Q. Li, R. Carpick, J.W. Kysar, J. Hone, Elastic and frictional properties of graphene, Phys. Status Solidi Basic Res. 246 (2009) 2562–2567. https://doi.org/10.1002/pssb.200982329.

[22] C. Lee, X. Wei, J.W. Kysar, J. Hone, Measurement of the elastic properties and intrinsic strength of monolayer graphene, Science (80-.). 321 (2008) 385–388. https://doi.org/10.1126/science.1157996.

[23] L. Gong, R.J. Young, I.A. Kinloch, I. Riaz, R. Jalil, K.S. Novoselov, Optimizing the

reinforcement of polymer-based nanocomposites by graphene, ACS Nano. 6 (2012) 2086–2095. https://doi.org/10.1021/nn203917d.

[24] H.O. Pierson, Handbook of Carbon, Graphite, Diamonds and Fullerenes, 1st ed., Noyes Publications, United States, 1993.

[25] Q. Zheng, Y. Geng, S. Wang, Z. Li, J.K. Kim, Effects of functional groups on the mechanical and wrinkling properties of graphene sheets, Carbon N. Y. 48 (2010) 4315–4322. https://doi.org/10.1016/j.carbon.2010.07.044.

[26] Z.M. Dang, L. Wang, Y. Yin, Q. Zhang, Q.Q. Lei, Giant dielectric permittivities in functionalized carbon-nanotube/ electroactive-polymer nanocomposites, Adv. Mater. 19 (2007) 852–857. https://doi.org/10.1002/adma.200600703.

[27] L.A. Fredin, Z. Li, M.T. Lanagan, M.A. Ratner, T.J. Marks, Substantial recoverable energy storage in percolative metallic aluminum-polypropylene nanocomposites, Adv. Funct. Mater. 23 (2013) 3560–3569. https://doi.org/10.1002/adfm.201202469.

[28] A.. Marsden, D.. Papageorgiou, C. Vallé, A. Liscio, V. Palermo, M.. Bissett, J. Young, R, I.A. Kinloch, Electrical percolation in graphene – polymer composites, 2D Mater. 5 (2018) 1–19. https://doi.org/10.1088/2053-1583/aac055.

[29] D. Stauffer, A. Amnon, Introduction to percolation theory, 2nd ed., Taylor & Francis Ltd, London, 1994.

[30] V. Myroshnychenko, C. Brosseau, Effective complex permittivity of two-phase random composite media: A test of the two exponent phenomenological percolation equation, J. Appl. Phys. 103 (2008) 1–10. https://doi.org/10.1063/1.2907769.

[31] D.M. Grannan, J.C. Garland, D.B. Tanner, Critical behavior of the dielectric constant of a random compostie near the percolation threshold, Phys. Rev. Lett. 46 (1980) 375–378. https://doi.org/10.1103/PhysRevLett.46.375.

[32] C.W. Nan, Physics of inhomogeneous inorganic materials, Prog. Mater. Sci. 37 (1993) 1–116. https://doi.org/10.1016/0079-6425(93)90004-5.

[33] S. El Bouazzaoui, A. Droussi, M.E. Achour, C. Brosseau, Nonuniversal percolation exponents and broadband dielectric relaxation in carbon black loaded epoxy composites, J. Appl. Phys. 106 (2009) 104107. https://doi.org/10.1063/1.3253744.

[34] A.K. Jonscher, The “universal” dielectric response, Nature. 267 (1977) 673–679. https://doi.org/10.1038/267673a0.

[35] Z. Li, B. Du, C. Han, H. Xu, Trap modulated charge carrier transport in polyethylene/graphene nanocomposites, Sci. Rep. 7 (2017) 1–8. https://doi.org/10.1038/s41598-017-04196-5.

[36] A.N. Papathanassiou, I. Sakellis, J. Grammatikakis, Universal frequency-dependent ac conductivity of conducting polymer networks, Appl. Phys. Lett. 91 (2007) 2005–2008. https://doi.org/10.1063/1.2779255.

[37] A.A. Khurram, S.A. Rakha, P. Zhou, M. Shafi, A. Munir, Correlation of electrical conductivity, dielectric properties, microwave absorption, and matrix properties of composites filled with graphene nanoplatelets and carbon nanotubes, J. Appl. Phys. 118 (2015) 044105. https://doi.org/10.1063/1.4927617.

[38] N.G. McCrum, B.E. Read, G. Williams, Anelastic and dielectric effects in polymeric solids, Wiley, London and New York, 1967.

[39] L. V. Karabanova, G. Boiteux, G. Seytre, I. Stevenson, O. Gain, C. Hakme, E.D. Lutsyk, A. Svyatyna, Semi-interpenetrating polymer networks based on polyurethane and poly(2-hydroxyethyl methacrylate): Dielectric study of relaxation behavior, J. Non. Cryst. Solids. 355 (2009) 1453–1460. https://doi.org/10.1016/j.jnoncrysol.2009.05.002.

[40] A.M. Castagna, D. Fragiadakis, H. Lee, T. Choi, J. Runt, The role of hard segment content on the molecular dynamics of poly(tetramethylene oxide)-based polyurethane copolymers, Macromolecules. 44 (2011) 7831–7836. https://doi.org/10.1021/ma2017138.

[41] S. Havriliak, S. Negami, A complex plane analysis of α-dispersions in some polymer systems, J. Polym. Sci. Part C Polym. Symp. 14 (1966) 99–117.

https://doi.org/10.1002/polc.5070140111.

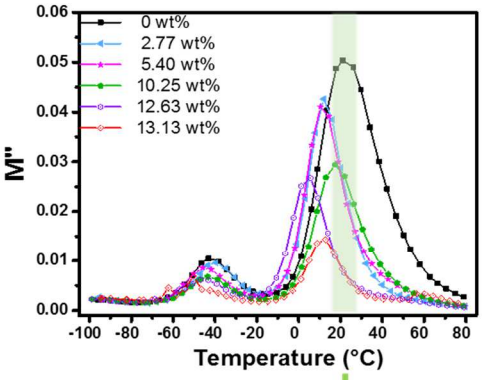
0 wt%
2.77 wt%
5.40 wt%
10.25 wt%
12.63 wt%
13.13 wt%
M''
Temperature (°C)

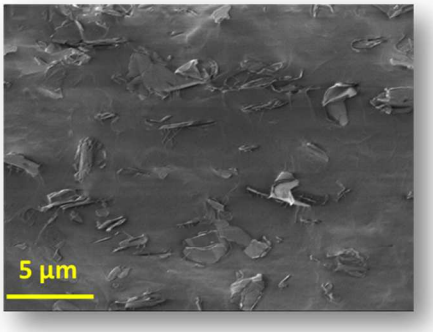
5 µm

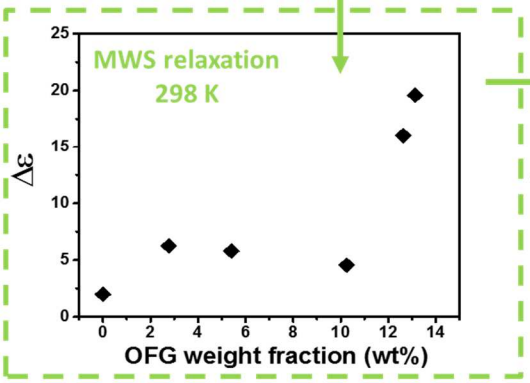
MWS relaxation
298 K
Δε
OFG weight fraction (wt%)

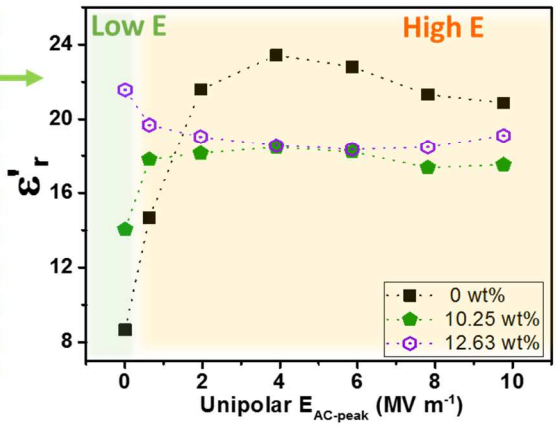
Low E
High E
ε'r
0 wt%
10.25 wt%
12.63 wt%
Unipolar E AC-peak (MV m-1)